














Relative velocities between ¹³CO structures within ¹²CO Molecular Clouds

LIXIA YUAN ¹, JI YANG ¹, XUEPENG CHEN ¹, YANG SU ¹, SHAOBO ZHANG ¹, XIN ZHOU ¹, ZHIWEI CHEN ¹,
QING-ZENG YAN ¹, MIN FANG ¹, FUJUN DU ¹, YAN SUN ¹, HONGCHI WANG ¹ AND YE XU ¹

¹*Purple Mountain Observatory and Key Laboratory of Radio Astronomy, Chinese Academy of Sciences,
10 Yuanhua Road, Qixia District, Nanjing 210033, PR China*

ABSTRACT

Velocity fields of molecular clouds (MCs) can provide crucial information on the merger and split between clouds, as well as their internal kinematics and maintenance, energy injection and redistribution, even star formation within clouds. Using the CO spectral lines data from the Milky Way Imaging Scroll Painting (MWISP) survey, we measure the relative velocities along the line of sight (ΔV_{LOS}) between ¹³CO structures within ¹²CO MCs. Emphasizing MCs with double and triple ¹³CO structures, we find that approximately 70% of ΔV_{LOS} values are less than $\sim 1 \text{ km s}^{-1}$, and roughly 10% of values exceed 2 km s^{-1} , with a maximum of $\sim 5 \text{ km s}^{-1}$. Additionally, we compare ΔV_{LOS} with the internal velocity dispersion of ¹³CO structures ($\sigma_{^{13}\text{CO},\text{in}}$) and find that about 40% of samples in either double or triple regime display distinct velocity discontinuities, i.e. the relative velocities between ¹³CO structures are larger than the internal linewidths of ¹³CO structures. Among these 40% samples in the triple regime, 33% exhibit signatures of combinations through the two-body motion, whereas the remaining 7% show features of configurations through the multiple-body motion. The ΔV_{LOS} distributions for MCs with double and triple ¹³CO structures are similar, as well as their $\Delta V_{\text{LOS}}/\sigma_{^{13}\text{CO},\text{in}}$ distributions. This suggests that relative motions of ¹³CO structures within MCs are random and independent of cloud complexities and scales.

Keywords: Interstellar medium(847) — Interstellar molecules(849) — Molecular clouds(1072)

1. INTRODUCTION

Molecular clouds are not isolated systems, but rather part of a network spanning from the warm diffuse ISM to the cold and dense molecular clouds. The dynamic evolution of these clouds can be characterized by two aspects: (1) Internally, hierarchical structures form within clouds, potentially leading to the formation of stars in gravitationally bound substructures; until, eventually, stellar feedback disperses the clouds (Larson 1981; Myers 1983; McKee 1989; Ballesteros-Paredes et al. 1999a; Mac Low & Klessen 2004; Molinari et al. 2010; André et al. 2010, 2014; Yuan et al. 2020). (2) Externally, mergers or splits between MCs and flows of gas in and out of the atomic phase can transfer mass, energy, and

momentum, altering the properties of clouds (Tasker & Tan 2009; Dobbs et al. 2011; Dobbs & Pringle 2013; Dobbs et al. 2015; Fukui et al. 2016; Gong et al. 2017; Fukui et al. 2018, 2021; Jeffreson et al. 2021; Skarbinski et al. 2023; Jeffreson et al. 2024). Molecular clouds thus undergo a range of dynamical processes, from the large-scale differential rotation and shearing motions to the sub-cloud dynamics associated with star formation and feedback (Ballesteros-Paredes et al. 2020; Henshaw et al. 2020). The possible driving forces, such as the thermal instability (Field 1965; Koyama & Inutsuka 2000), converging flows (Vázquez-Semadeni et al. 1995; Paspot et al. 1995; Ballesteros-Paredes et al. 1999b; Heitsch et al. 2006; Beuther et al. 2020), gravity (Lin & Shu 1964; Goldreich & Lynden-Bell 1965; Vázquez-Semadeni et al. 2007; Traficante et al. 2020), and magnetic fields (Chandrasekhar & Fermi 1953; Shu et al. 1987; Myers & Goodman 1988; Vázquez-Semadeni et al. 2011; Li & Burkert 2018) likely play a role at various stages of these processes. However, the details of the MC evolution,

Corresponding author: Ji Yang

jiyang@pmo.ac.cn

lx yuan@pmo.ac.cn

both internally and externally, remain incompletely understood.

The properties of MCs have been extensively researched and analyzed in the literature. This includes their masses, sizes, velocity dispersion, etc., and the scaling relations between cloud sizes, velocity dispersion, surface densities, etc. (e.g. Larson 1981; Dame et al. 1986; Solomon et al. 1987; Heyer et al. 2009; Roman-Duval et al. 2010; Rice et al. 2016; Miville-Deschênes et al. 2017; Riener et al. 2020; Rani et al. 2023). Moreover, the column density probability distribution (e.g. Vazquez-Semadeni 1994; Ma et al. 2021, 2022) and the velocity structure function (e.g. Heyer & Brunt 2004; Heyer et al. 2006) are also used to investigate the distributions of column densities and velocity fields in MCs. These studies provide a comprehensive understanding of the kinematic, dynamic, structural, and evolutionary characteristics of MCs.

Our recent series of studies based on a large sample of MCs from the Milky Way Imaging Scroll Painting (MWISIP) CO survey (Su et al. 2019), find that as MCs grow in scale, they tend to exhibit more complex filamentary networks (Yuan et al. 2021, hereafter Paper I) and host greater numbers of ^{13}CO structures (Yuan et al. 2022, hereafter Paper II). These ^{13}CO structures have areas that generally do not exceed 70% of the MC's ^{12}CO emission areas (Paper II). In addition, we revealed a preferred spatial separation among individual ^{13}CO structures, which is independent of the MC's scale (Yuan et al. 2023a, hereafter Paper III). Furthermore, we found that the relative motions between ^{13}CO structures are the primary contributor to the total velocity dispersions of MCs (Yuan et al. 2023b, hereafter Paper IV). Based on these observed results, an alternative picture for the assembly and destruction of MCs has been proposed. It suggests that the regularly spaced ^{13}CO structures serve as the building blocks for MCs, and the transient processes of MCs occur through slow mergers or splits among these fundamental blocks. Meanwhile, these processes do not significantly alter MCs' density structures but do affect their global velocity fields. Numerical models indicate that mergers between clouds are gentle and do not heavily impact the density structures of clouds, but they can result in higher velocity dispersions of MCs (Dobbs et al. 2011, 2015; Jeffreson et al. 2021; Skarbinski et al. 2023), which are consistent with our pictures.

The picture above provides crucial insights into the build-up process of MC. It is mainly based on the spatial distribution and motions of internal ^{13}CO structures. The motions of gas displays distinct characteristics, such as noticeable variations in velocity, which likely result from the process of merging or splitting. ^{13}CO struc-

tures are considered as the fundamental building blocks of material transfer between clouds as described in Paper III and Paper IV. By analyzing velocity fields of ^{13}CO structures within clouds, we can gain key clues to resolve the gas motions within clouds and better understand the material transfer processes between clouds. It also sheds light on the energy injection sources driving the kinematics of MCs, and the processes of energy redistribution and material gathering for star formation.

In this research, we focus on the relative velocities of the ^{13}CO structures. This paper is organized as follows: Section 2 presents the data from the MWISIP CO survey, along with the identification of ^{12}CO molecular clouds and their harbored ^{13}CO structures. Section 3 mainly describes the results, including the distributions of line-of-sight relative velocities between ^{13}CO structures within MCs, as well as ratios between relative velocities and velocity dispersions of ^{13}CO structures within MCs, the fractions of MCs displaying distinct velocity discontinuities. In Section 4, we discuss the observational bias in our results and compare our observed results with previously simulated works. Section 5 summarizes our findings.

2. DATA

2.1. *The $^{12}\text{CO}(J=1-0)$ and $^{13}\text{CO}(J=1-0)$ spectral lines data from the MWISIP survey*

The Milky Way Imaging Scroll Painting (MWISIP) survey is an ongoing northern Galactic plane CO survey, which is performed by the 13.7m telescope at Delingha, China, and observes the ^{12}CO , ^{13}CO , and C^{18}O lines at the transition $J=1-0$, simultaneously. A detailed description of the performance of the telescope and its 3×3 multibeam sideband-separating Superconducting Spectroscopic Array Receiver (SSAR) system is given in Su et al. (2019); Shan et al. (2012). The observational strategy and raw data processing are also introduced in Su et al. (2019). The half-power beamwidth (HPBW) of the antenna at the frequencies of 115 GHz is $\sim 50''$. The typical system temperature is ~ 250 K at a line frequency of the ^{12}CO line (115.271 GHz) in the upper sideband and ~ 140 K at ^{13}CO (110.201 GHz) and C^{18}O (109.782 GHz) lines in the lower sideband, respectively. The total bandwidth of 1 GHz with 16,384 channels provides a spectral resolution of 61 kHz per channel, resulting in a velocity resolution of about 0.16 km s^{-1} for ^{12}CO lines and 0.17 km s^{-1} for ^{13}CO and C^{18}O lines. The typical RMS achieved in ^{12}CO and ^{13}CO lines are ~ 0.5 K and ~ 0.3 K, respectively.

In this work, the ^{12}CO and ^{13}CO lines data are from the MWISIP survey and cover about 450 deg^2 region with the Galactical longitude l from $104^\circ.75$ to $150^\circ.25$, the

Galactical latitude $|b| < 5^\circ.25$, and the line-of-sight velocity of $-95 \text{ km s}^{-1} < V_{\text{LSR}} < 25 \text{ km s}^{-1}$. These ^{12}CO and ^{13}CO lines emission data also have been analyzed in our previous series of works in Yuan et al. (2021, 2022, 2023a,b).

2.2. The ^{12}CO molecular clouds and their internal ^{13}CO structures

In our analysis, the ^{12}CO molecular cloud is defined as a set of adjacent voxels in the position-position-velocity (PPV) space with observed $^{12}\text{CO}(1-0)$ line intensities exceeding a certain threshold. The Density-based Spatial Clustering of Applications with Noise (DBSCAN) algorithm, designed to discover clusters with arbitrary shapes in large spatial databases (Ester et al. 1996), was employed to identify MCs in the ^{12}CO data cube by Yan et al. (2020). This algorithm combines both intensity levels and continuity of signals, which is appropriate for the extended and irregular shapes of MCs. Three parameters are used in the DBSCAN to extract the ^{12}CO MCs, one parameter of *cutoff* determines the line intensity threshold, while the other two parameters of ϵ and *MinPts* define the connectivity of the extracted structures. A core point within extracted structures satisfies that its adjacent points within a certain radius (ϵ) have to exceed a threshold number (*MinPts*). The border point is inside the ϵ -radius of a core point, but its adjacent points within the radius of ϵ do not exceed the number of *MinPts* (Yan et al. 2020). The parameters of *cut-off*= 2σ (σ is the rms noise, whose value is $\sim 0.5 \text{ K}$ for the ^{12}CO line emission), *MinPts*=4, and ϵ =1 are used for the identification of ^{12}CO clouds, as suggested in (Yan et al. 2020). Moreover, post-selection criteria are utilized to avoid noise contamination, which includes: (1) the total number of voxels in each extracted structure is greater than 16; (2) the peak intensity of extracted voxels must be higher than the *cutoff* value adding 3σ ; (3) the angular area of the extracted structure must be larger than one beam size (2×2 pixels $\sim 1'$); and (4) the number of velocity channels must be greater than 3. Using aforementioned parameters and criteria, a catalog of 18,190 ^{12}CO molecular clouds was identified in the above region by the DBSCAN algorithm (Yan et al. 2021). We have visually inspected and classified these 18,190 MCs into filaments and nonfilaments in Paper I. Additionally, the dependence of extracted MC samples on the finite angular resolution, sensitivity of observed spectral lines, and different algorithms have been systematically investigated in Yan et al. (2022).

Individual ^{13}CO structures are defined as connected voxels in the PPV space, meanwhile the ^{13}CO line intensities on these voxels must exceed a certain thresh-

Table 1. Number of MC sources in different groups.

Group	Sources	Sources in Near	Sources in Far
All	2851	988	1863
Single	1848	576	1272
Double	443	163	280
Triple	185	80	105

old. We have extracted the ^{13}CO structures within the boundaries of ^{12}CO MCs using the DBSCAN algorithm. The utilized parameters are same with the parameters for ^{12}CO MC identification, with the exception of the post-selection criteria of the peak intensities exceeding the *cutoff* value adding 2σ , where σ is $\sim 0.25 \text{ K}$ for ^{13}CO spectral lines. Among a total of 18,190 ^{12}CO clouds, 2851 ^{12}CO clouds are identified to harbor the ^{13}CO structures (Paper II). We have presented the distributions of the physical properties of these extracted ^{13}CO structures in Paper II and III. Among our 2851 MCs having ^{13}CO structures, 1848 (64.8%) MCs have a single ^{13}CO structure, 443 (15.5%) MCs have double ^{13}CO structures, 185 (6.5%) MCs have triple ^{13}CO structures, the rest (13.2%) have more than three ^{13}CO structures, as listed in Table 1.

In addition, according to the spiral structure model of the Milky Way (Reid et al. 2016, 2019; Xu et al. 2023), the MC samples are further divided into two groups, i.e., near and far. The MC samples in the near group have central velocities ranging from -30 to 25 km s^{-1} , which are mainly distributed in the local arm and have kinematical distances of $\sim 0.5 \text{ kpc}$. The MC samples in the far group have central velocities in a range of $(-95$ to $-30) \text{ km s}^{-1}$, most of which are located in the Perseus arm and their kinematical distances concentrate on $\sim 2 \text{ kpc}$ (Reid et al. 2016). Considering these kinematical distances, the physical scale for the MC with an angular size of $1'$ in the local arm is about 0.15 pc , and this value is $\sim 0.6 \text{ pc}$ for that in the Perseus arm. The number of MC samples distributed in the near and far groups has also been listed in Table 1.

3. RELATIVE VELOCITIES BETWEEN ^{13}CO STRUCTURES WITHIN MOLECULAR CLOUDS

In our previous studies (Paper III and IV), we have proposed that regularly spaced ^{13}CO structures serve as the fundamental units of the gas transfer between clouds. Additionally, mergers or splits between clouds

have an impact on their velocity fields, resulting in two distinct features: (1) relatively discontinuous velocity fields with blue and redshifted velocities, and (2) velocity structures with two or more velocity components, leading to higher velocity dispersions. Based on these features, we aim to investigate the relative velocities between individual ^{13}CO structures within MCs and the imprints on the build-up processes of MCs they provide.

To achieve this, we first determine the relative velocities between each pair of ^{13}CO structures within the MCs. The relative velocities between ^{13}CO structures are defined as the absolute differences between their centroid velocities. Thus the relative velocity (ΔV_{LOS}) between j th and $(j-1)$ th ^{13}CO structures along the line of sight can be calculated as:

$$\Delta V_{j,j-1} = \left| V_{\text{cen},^{13}\text{CO},j} - V_{\text{cen},^{13}\text{CO},j-1} \right|$$

$$V_{\text{cen},^{13}\text{CO},j} = \frac{\sum_i^{j\text{th}} T_{13\text{CO},ji} V_{13\text{CO},ji}}{\sum_i^{j\text{th}} T_{13\text{CO},ji}}, \quad (1)$$

where $V_{\text{cen},^{13}\text{CO},j}$ represents the centroid velocity of the j th ^{13}CO structure, the sum $\sum_i^{j\text{th}}$ runs over all voxels within the j th ^{13}CO structure, the $T_{13\text{CO},ji}$ and $V_{13\text{CO},ji}$ are the brightness temperature and line-of-sight velocity of ^{13}CO emission at the i th voxel in the j th ^{13}CO structure.

Secondly, we compare the relative velocities with the internal velocity dispersion of ^{13}CO structures. The internal velocity dispersion of ^{13}CO structures ($\sigma_{13\text{CO},\text{in}}$) within a cloud are defined as:

$$\sigma_{13\text{CO},\text{in}}^2 = \frac{\sum_j^{\text{cloud}} F_{13\text{CO},j} \sigma_{13\text{CO},j}^2}{\sum_j^{\text{cloud}} F_{13\text{CO},j}},$$

$$\sigma_{13\text{CO},j}^2 = \frac{\sum_i^{j\text{th}} T_{13\text{CO},ji} (V_{13\text{CO},ji} - V_{\text{cen},^{13}\text{CO},j})^2}{\sum_i^{j\text{th}} T_{13\text{CO},ji}}, \quad (2)$$

where the sum \sum_j^{cloud} runs over the whole individual ^{13}CO structures within a ^{12}CO cloud, the $\sigma_{13\text{CO},j}$ is the velocity dispersion within the j th ^{13}CO structure, $F_{13\text{CO},j} = \int T_{mb}(l, b, v) dl db dv = 0.167 \times 0.25 \sum_i^{j\text{th}} T_{13\text{CO},ji}$ ($\text{K km s}^{-1} \text{ arcmin}^2$) is the integrated flux of ^{13}CO line emission for the j th ^{13}CO structure.

Furthermore, if the relative velocities between ^{13}CO structures within a cloud satisfy:

$$\Delta V_{\text{LOS}} > \sqrt{8 \ln 2} \sigma_{13\text{CO},\text{in}} \quad (3)$$

i.e. the relative velocities between ^{13}CO structures are greater than the internal linewidth of ^{13}CO structures, they are characterized as the distinct velocity discontinuities (ΔV_{dis}).

3.1. Molecular clouds with double ^{13}CO structures

Each MC with double ^{13}CO structures has a single ΔV_{LOS} , as illustrated in Figure 1, making it easier to analyse the relative movement between ^{13}CO structures within a cloud. Here we focus on the 443 MC samples with double ^{13}CO structures, whose physical properties are shown in Figures A1 and A2. Based on the kinematical distances of these clouds, the interquartile ranges of their physical scales are 1 – 2 pc for those in the near group and 3.5 – 5.6 pc for the far group.

Figure 2 presents the distributions of ΔV_{LOS} and $\Delta V_{\text{LOS}}/\sigma_{13\text{CO},\text{in}}$ ratios for these MCs. The quantiles at 0.05, 0.25, 0.5, 0.75, and 0.95 and the mean values of the ΔV_{LOS} and $\Delta V_{\text{LOS}}/\sigma_{13\text{CO},\text{in}}$ are listed in Tables 2 and 3, respectively. Approximately 70% of ΔV_{LOS} in the ‘Double’ samples are less than 1 km s^{-1} , with less than 10% having values greater than 2 km s^{-1} and reaching a maximal value of approximately 5 km s^{-1} . The distributions of ΔV_{LOS} in the near and far groups have similar patterns, but the greater ΔV_{LOS} ($3 - 5 \text{ km s}^{-1}$) have slightly higher probabilities to be observed in the far group. The quantiles of ΔV_{LOS} in the far group are ~ 1.3 times greater than those in the near group, probably due to the beam dilution effects on clouds with different distances, as previously discussed in Section 4.1 in Paper III, which also cause the linear separations among ^{13}CO structures in the far group to be ~ 3 times those in the near group.

For the distribution of $\Delta V_{\text{LOS}}/\sigma_{13\text{CO},\text{in}}$, approximately 50% of values are less than 2, and around 70% are less than 3. About 10% of samples exhibit $\Delta V_{\text{LOS}}/\sigma_{13\text{CO},\text{in}}$ greater than 5, with several samples reaching ~ 12 . The ratio values ($\Delta V_{\text{LOS}}/\sigma_{13\text{CO},\text{in}}$) and their quantiles for the samples in the near and far groups display consistent distributions. Among these clouds, about 42% of ΔV_{LOS} are identified as distinct velocity discontinuities (ΔV_{dis}), where $\Delta V_{\text{dis}} > \sqrt{8 \ln 2} \sigma_{13\text{CO},\text{in}}$, as listed in Table 4. We also visually examine the velocity fields for these clouds with ΔV_{dis} , whose velocity fields are derived from the first moment of the ^{12}CO and ^{13}CO line emission, and present their averaged spectral lines of ^{12}CO and ^{13}CO line emission. The velocity fields of these clouds exhibit the following features: (1) relatively discontinuities on velocity fields, with one ^{13}CO structure displaying blueshifted velocity and the other redshifted; (2) the averaged ^{13}CO spectral lines resolving into two velocity components, as shown in several cases in Figure B1. Based on these observations, about 42% of MCs in the ‘double’ regime show the signs of ongoing mergers or splits between clouds.

3.2. Molecular clouds with triple ^{13}CO structures

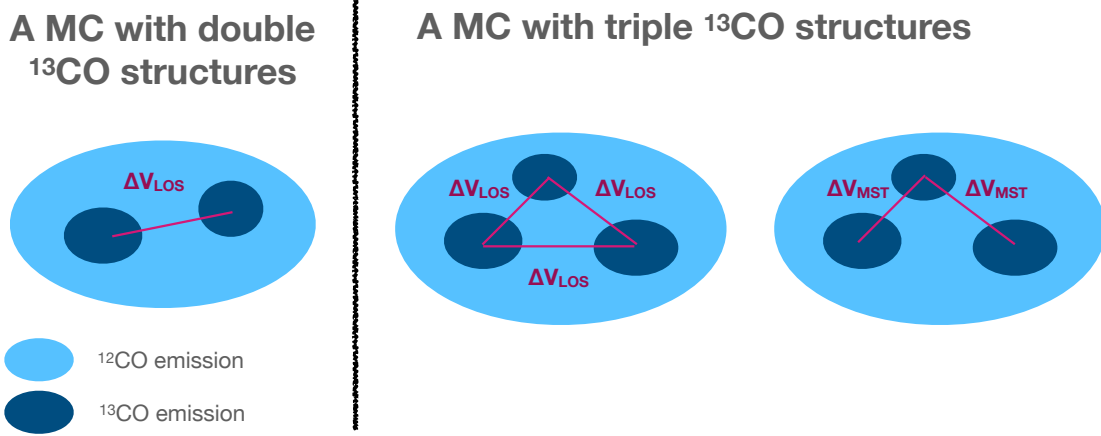


Figure 1. Relative velocities along the line of sight between ^{13}CO structures (ΔV_{LOS}) in MCs with double and triple ^{13}CO structures. A single MC with double ^{13}CO structures has one ΔV_{LOS} . A single MC with triple ^{13}CO structures have three ΔV_{LOS} between each two ^{13}CO structures or two ΔV_{MST} between each pair of ^{13}CO structures connected by the minimal spanning tree (MST) algorithm.

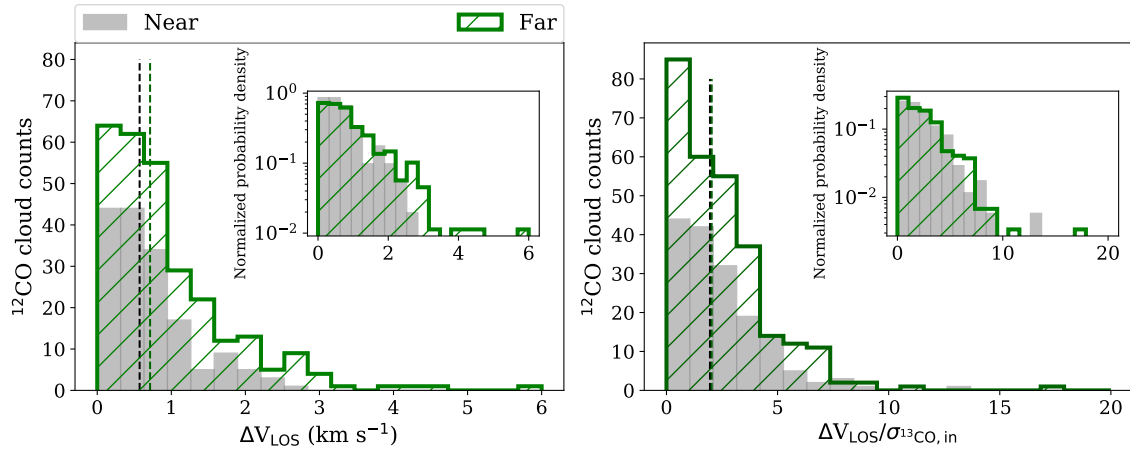


Figure 2. Number distributions of the relative velocities (ΔV_{LOS}) and their ratios with internal velocity dispersions of ^{13}CO structures ($\Delta V_{\text{LOS}}/\sigma_{^{13}\text{CO},\text{in}}$) for MCs with double ^{13}CO structures. The ‘Near’ represents MCs have central velocities ranging from -30 to 25 km s^{-1} , the ‘Far’ means clouds with central velocities in a range of -95 to -30 km s^{-1} . The vertical-dashed lines denote the corresponding median values. In the upper-right corner of each panel, the corresponding normalized probability densities are presented. The normalized probability densities are presented as log scales, and the values in x-axis are binned as linear scales.

As mentioned above, approximately 20% of the whole MC samples contain more than two ^{13}CO structures. The analysis of relative velocities between multiple ^{13}CO structures becomes increasingly complex as the number of ^{13}CO structures increases. Here we focus on the 185 MC samples with triple ^{13}CO structures, whose physical properties are presented in Figures A1 and A2. Based on the kinematical distances of these clouds, the interquartile ranges of their physical scales are $1.5 - 2.5 \text{ pc}$ for those in the near group and $4.7 - 7.0 \text{ pc}$ for the far group.

3.2.1. Relative velocities between each two ^{13}CO structures

An individual MC with triple ^{13}CO structures contains three ΔV_{LOS} values between each two ^{13}CO structures, as illustrated in Figure 1. The distributions of the ΔV_{LOS} values within these MC samples in both near and far groups are presented in Figure 3. The distributions of their maximum ΔV_{LOS} (ΔV_{max}) within each sample are also presented, along with the quantiles at 0.05, 0.25, 0.5, 0.75, and 0.95, and the mean values of the ΔV_{LOS} and ΔV_{max} , which are tabulated in Table 2. We find that the distributions of ΔV_{LOS} in the MCs in the ‘triple’ and ‘double’ regimes are similar, and their quantiles and mean values are also close for both near and far groups. However, the ΔV_{max} , whose median value

is about 0.92 km s^{-1} in the near group and 1.3 km s^{-1} in the far group, is significantly larger than those values for MCs in the ‘double’ regime. It should be noted that ΔV_{max} is the maximum value for the ΔV_{LOS} between each pair of the ^{13}CO structures. Therefore, the larger ΔV_{max} is likely due to statistical probabilities for the larger number of the ^{13}CO structure pairs in the ‘triple’ regime.

Figure 3 displays distribution of the ratios between the ΔV_{LOS} with $\sigma_{^{13}\text{CO},\text{in}}$ and the ratios between ΔV_{max} and $\sigma_{^{13}\text{CO},\text{in}}$ for MCs with triple ^{13}CO structures. In Table 3, the quantiles at 0.05, 0.25, 0.5, 0.75, and 0.95, as well as the mean values of these $\Delta V_{\text{LOS}}/\sigma_{^{13}\text{CO},\text{in}}$ and $\Delta V_{\text{max}}/\sigma_{^{13}\text{CO},\text{in}}$ values, are also listed. The distributions of $\Delta V_{\text{LOS}}/\sigma_{^{13}\text{CO},\text{in}}$ for MCs with triple ^{13}CO structures are remarkably similar to those for MCs with double ^{13}CO structures, with a nearly consistent interquartile range of $\sim 0.9 - 3.4$ and a median value of ~ 2 , in either the near or far group. However, the $\Delta V_{\text{max}}/\sigma_{^{13}\text{CO},\text{in}}$ values in the near group (median value of 3.26) and far group (median value of 2.77) are significantly greater than those values in MCs with double ^{13}CO structures, which can be attributed to the greater ΔV_{max} . Overall, the distributions of the ΔV_{LOS} for both ‘double’ and ‘triple’ regime samples are similar, as well as their $\Delta V_{\text{LOS}}/\sigma_{^{13}\text{CO},\text{in}}$ distributions. Such similarities suggest that the relative motions of ^{13}CO structures within clouds are regulated by the fundamental processes that are independent of structure complexities and cloud scales.

3.2.2. Relative velocities between ^{13}CO structures connected by MST

For a cloud containing three ^{13}CO structures, the relative velocities between each pair of them do not take the spatial distribution of ^{13}CO structures into account. In order to examine whether the relative motion between ^{13}CO structures is primarily random motion or systematic motion, we connect the centroid coordinates of ^{13}CO structures together using the minimal spanning tree (MST), which minimizes the sum of the angular separation between ^{13}CO structures. Furthermore, we analyzed the relative velocities (ΔV_{MST}) between the connected ^{13}CO structures. There are two ΔV_{MST} values in each MC with triple ^{13}CO structures, as illustrated in Figure 1.

The distributions of ΔV_{LOS} and ΔV_{MST} for the 185 MCs in the triple regime, are showed in Figure 4. We find that their distributions are nearly accordant, espe-

cially for their normalized probability densities. Such similarity means the relative motions between ^{13}CO structures are random and regulated by fundamental processes. Turbulent flows are a promising candidate for this process, as they are driven by dynamical processes in different scales, including galactic differential rotation and shear (Kim et al. 2006; Bonnell et al. 2006; Dobbs & Bonnell 2008), large-scale instabilities (Wada et al. 2002; Tasker & Tan 2009), and stellar feedback from the supernova explosions (Brunt et al. 2009; Skarbinski et al. 2023; Watkins et al. 2023) and HII regions (Silk 1985; Krumholz et al. 2006).

3.2.3. Distinct velocity discontinuities within MCs

Among 185 MCs with triple ^{13}CO structures, 21.1% of these MCs have one ΔV_{dis} , 33.5% of samples exhibit two ΔV_{dis} , and 7% of them display three ΔV_{dis} , as listed in Table 4. We further conducted visual inspections of the velocity fields (first moment maps of CO emission) of these clouds and the averaged spectral lines of their ^{12}CO and ^{13}CO emissions. In Figure B2, we present the velocity fields for clouds with two ΔV_{dis} , which have two ^{13}CO structures with redshifted (blueshifted) velocities, and the other ^{13}CO structure exhibits blueshifted (redshifted) velocities. Furthermore, the averaged spectra of ^{13}CO emission are resolved into two velocity components. Figure B3 shows the velocity fields for clouds with three ΔV_{dis} , featuring three different velocity fields, each harboring one ^{13}CO structure. The averaged spectra of ^{13}CO emission are also decomposed into three velocity components.

We suggest that the build-up processes for MCs containing triple ^{13}CO structures could be a result of two clouds combination, one with double ^{13}CO structures and the other with single ^{13}CO structure (two-body mode), or the assembly of three clouds, each with a single ^{13}CO structure (multiple-body mode). Figure 5 illustrates the velocity fields of cloud interaction through two-body and multiple-body modes, respectively. In the two-body mode, one ^{13}CO structure exhibits redshifted (blueshifted) velocity, while the other two ^{13}CO structures display the blueshifted (redshifted) velocity, with two ΔV_{dis} between one ^{13}CO structure and the other two ^{13}CO structures within clouds. In the multiple-body mode, each ^{13}CO structure has a distinct velocity, resulting in three discontinuous velocity fields in the cloud’s velocity fields. Thus three ΔV_{dis} between each pair of ^{13}CO structures are expected within the cloud. That is, the velocity fields of clouds are constructed by velocities from these ^{13}CO structures and exhibit three discontinuous velocities.

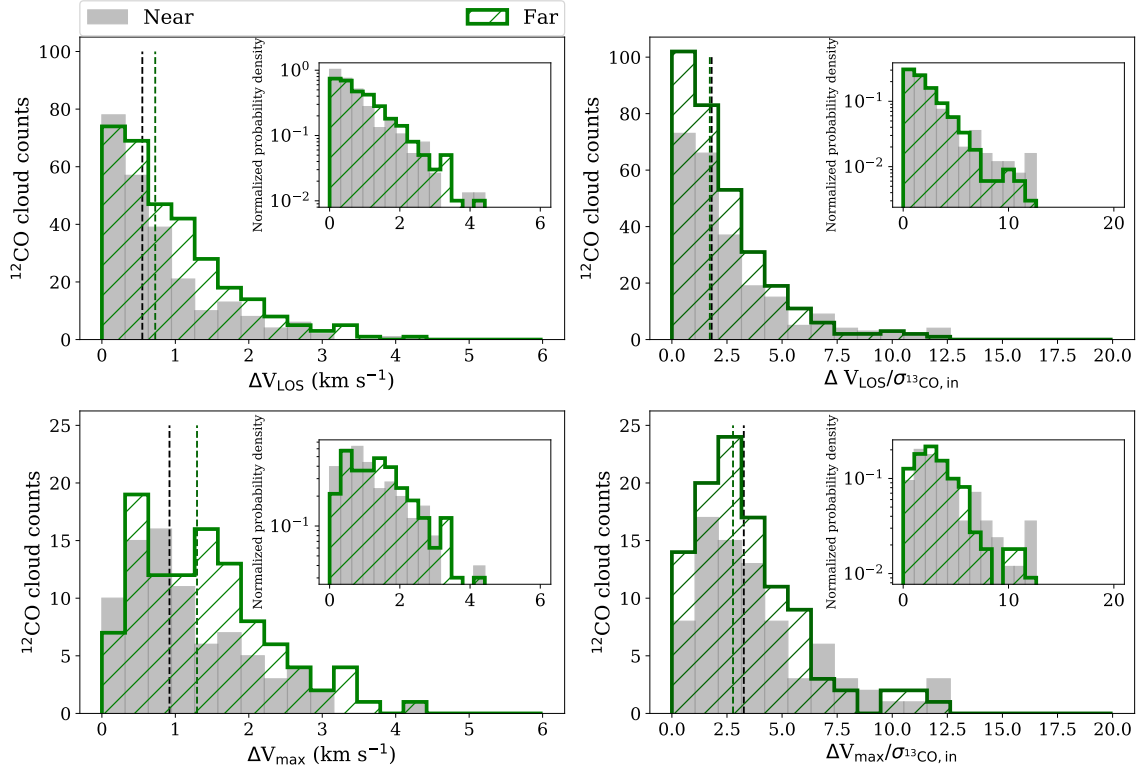


Figure 3. Upper panel: number distributions of relative velocities (ΔV_{LOS}) between each two ^{13}CO structures in the MC samples having triple ^{13}CO structures and their ratios with internal velocity dispersions of ^{13}CO structures ($\Delta V_{\text{LOS}}/\sigma_{^{13}\text{CO},\text{in}}$). **Lower panel:** number distributions of the maximum relative velocity (ΔV_{max}) within each MC and their ratios with internal velocity dispersions ($\Delta V_{\text{max}}/\sigma_{^{13}\text{CO},\text{in}}$). The vertical-dashed lines show their median values. In the upper-right corner of each panel, the corresponding normalized probability densities are presented. The normalized probability densities are presented as log scales, and the values in x-axis are binned as linear scales.

Thus, in the ‘triple’ regime, about 40.5% of MCs show distinct velocity discontinuities, with 33.5% of clouds displaying the signatures of the two-body mode and only 7% of clouds presenting the multiple-body mode. This suggests that cloud mergers or splits tend to occur between two MCs. Horie et al. (2023) simulated the fraction of mass from each progenitor within a colliding GMC and found the sum of the two most significant fractions is mostly close to 1, also suggesting a two-body mode for the majority of MC collisions. We should note that 21.1% of MCs have one ΔV_{dis} between the arbitrary two ^{13}CO structures, but do not exhibit the distinct discontinuity in velocity field caused by the bulk motions of ^{13}CO structures. These clouds are not included into the MCs in triple regime showing distinct velocity discontinuities.

In summary, the similarity of the ΔV_{LOS} distribution in the double and triple regimes indicates the relative motion between ^{13}CO structures is random and independent of cloud scales. Additionally, a considerable portion of distinct velocity discontinuities between ^{13}CO structures (ΔV_{dis}) is observed within ^{12}CO MCs. These

results are coincident with our previous findings on regularly spaced ^{13}CO structures within MCs (Paper III) and distinctly demonstrate on how the relative motion of ^{13}CO structures provides a dominant contribution to the kinetic energy of MCs (Paper IV). Thus these results further support our previously proposed picture that ^{13}CO structures act as the building blocks of MCs, and the transient processes of MCs proceed by slow mergers or splits among these fundamental blocks.

4. DISCUSSION

4.1. Observational bias

Our observed MC samples are identified as the contiguous structures in the position-position-velocity (PPV) space, which have $^{12}\text{CO}(1-0)$ emission intensities above a certain threshold. However, it is important to note that the structure identification in the PPV intensity structures, compared with the real structures in the position-position-position (PPP), may have some bias due to the effects of projection. This bias is attributed to two main factors. Firstly, distinct structures in the

Table 2. Radial relative velocities (ΔV_{LOS}) between ^{13}CO structures within ^{12}CO MC samples.

Groups	MC samples	Relative velocities	0.05	0.25	0.5	0.75	0.95	Mean
Near	MCs (Double)	ΔV_{LOS}	0.05	0.28	0.57	0.95	1.93	0.75
	MCs (Triple)	ΔV_{LOS}	0.05	0.23	0.55	1.0	2.47	0.77
		ΔV_{max}	0.15	0.53	0.92	1.69	2.78	1.15
Far	MCs (Double)	ΔV_{LOS}	0.08	0.35	0.71	1.24	2.64	0.94
	MCs (Triple)	ΔV_{LOS}	0.08	0.33	0.73	1.29	2.47	0.93
		ΔV_{max}	0.29	0.67	1.3	1.89	3.14	1.39

NOTE—The quantiles at 0.05, 0.25, 0.5, 0.75, and 0.95 for the ΔV_{LOS} (km s^{-1}) in their sequential data. The ‘Double’ represents the 443 MCs with double ^{13}CO structures and the ‘Triple’ corresponds to the 185 MCs having three ^{13}CO structures. The ‘Near’ and ‘Far’ represent the MC samples in the near and far groups, respectively. The ΔV_{LOS} is the relative velocity on the line of sight between ^{13}CO structures. There is one ΔV_{LOS} in each ‘Double’ sample and three ΔV_{LOS} in each ‘Triple’ sample. The ‘ ΔV_{max} ’ means the maximum value in the three ΔV_{LOS} of each ‘Triple’ sample.

Table 3. The ratios between relative velocities and internal velocity dispersions ($\Delta V_{\text{LOS}}/\sigma_{^{13}\text{CO},\text{in}}$) of ^{13}CO structures within ^{12}CO MC samples.

Groups	MC samples	Ratios	0.05	0.25	0.5	0.75	0.95	Mean
Near	MCs (Double)	$\Delta V_{\text{LOS}}/\sigma_{^{13}\text{CO},\text{in}}$	0.28	0.97	1.96	3.41	5.93	2.43
	MCs (Triple)	$\Delta V_{\text{LOS}}/\sigma_{^{13}\text{CO},\text{in}}$	0.18	0.93	1.8	3.44	8.07	2.6
		$\Delta V_{\text{max}}/\sigma_{^{13}\text{CO},\text{in}}$	0.88	1.89	3.26	4.89	9.63	3.89
Far	MCs (Double)	$\Delta V_{\text{LOS}}/\sigma_{^{13}\text{CO},\text{in}}$	0.24	0.88	2.04	3.34	6.46	2.45
	MCs (Triple)	$\Delta V_{\text{LOS}}/\sigma_{^{13}\text{CO},\text{in}}$	0.22	0.77	1.72	3.09	6.2	2.29
		$\Delta V_{\text{max}}/\sigma_{^{13}\text{CO},\text{in}}$	0.62	1.85	2.77	4.69	7.97	3.44

NOTE—The quantiles at 0.05, 0.25, 0.5, 0.75, and 0.95 for the $\Delta V_{\text{LOS}}/\sigma_{^{13}\text{CO},\text{in}}$ and $\Delta V_{\text{max}}/\sigma_{^{13}\text{CO},\text{in}}$ in their sequential data. The MC samples are reported in Table 2.

Table 4. Fractions of MC samples with the distinct velocity discontinuities.

MC samples	Zero	One	Two	Three
MCs (Double)	58.2%	41.8%	- -	- -
MCs (Triple)	38.4%	21.1%	33.5%	7.0%

NOTE—The fractions of MCs not having the distinct velocity discontinuity (ΔV_{dis}) and having one ΔV_{dis} in MC samples with double ^{13}CO structures. Also, the fractions of MCs not having ΔV_{dis} (zero) and having one, two, and three ΔV_{dis} in MC samples with triple ^{13}CO structures.

PPP space that move at similar velocities along the line of sight can be projected as a contiguous structure in the PPV space. Secondly, a single structure in the PPP space that has distinct velocity gradients can result in multiple PPV structures. Unfortunately, these ambiguities that are caused by projection cannot be directly resolved through a simple method in observations. To mitigate this issue, we combine the observed and simulated results.

In observations, the number of velocity components per spectrum along the line of sight can give us a global insight into the level of velocity crowding in the observed region of sky. Our MC samples are located in the second Galactic quadrant with $l = 104^{\circ}.75 - 150^{\circ}.25$, $|b| < 5^{\circ}.25$, and $-95 \text{ km s}^{-1} < V_{\text{LSR}} < 25 \text{ km s}^{-1}$. In total, we have extracted 18,190 ^{12}CO clouds in the

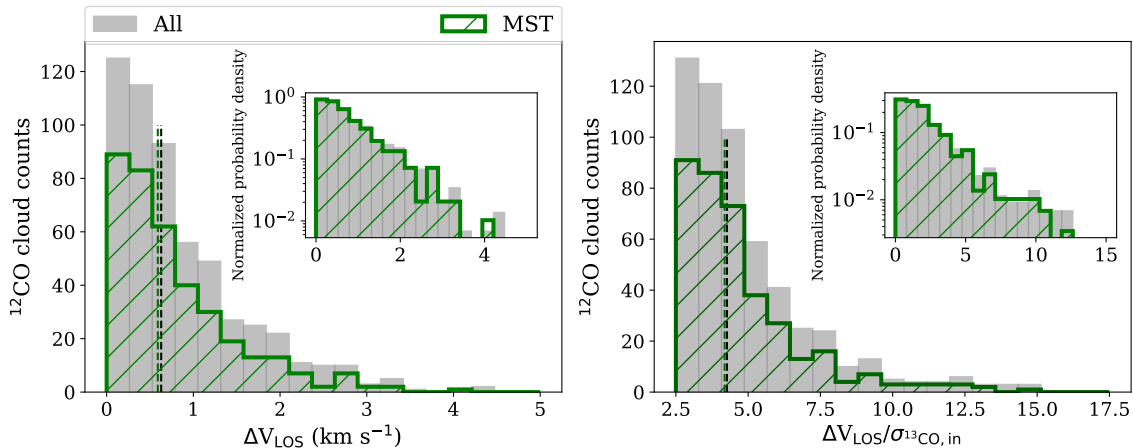


Figure 4. The distribution of relative velocities between ^{13}CO structures for 185 MCs in the ‘triple’ regime. The gray histograms represent the whole 555 ΔV_{LOS} from the arbitrary two of ^{13}CO structures within 185 samples. The green histograms mean the 370 ΔV_{MST} between the ^{13}CO structures connected through the minimal spanning three (MST) algorithm, there are two ΔV_{MST} within a cloud. The corresponding vertical-dashed lines show their median values. In the upper-right corner of each panel, the corresponding normalized probability densities are presented. The normalized probability densities are presented as log scales, and the values in x-axis are binned as linear scales.

PPV space of ^{12}CO emission within this region. Figure 6 shows the number distribution of 18,190 ^{12}CO clouds per line of sight. We find that on $\sim 40\%$ of this sky region, there is no cloud on the line of sight. In addition, on another $\sim 40\%$ of the region, there is only one cloud along the line of sight. In approximately 15% of this area, two clouds overlap on the line of sight, and $\sim 5\%$ of positions intersect three or four clouds. Furthermore, we count the number of molecular clouds along the line of sight, which are in the velocity range of $(-95 -30)$ km s^{-1} (Far) and $(-30 25)$ km s^{-1} (Near), respectively. As shown in Figure 6, approximately 50% of positions have no cloud and $\sim 40\%$ have only one cloud on the line of sight in the near range. However, on the line of sight in the far range, $\sim 85\%$ of areas have no cloud and $\sim 15\%$ have only one cloud. Additionally, [Riener et al. \(2020\)](#); [Miville-Deschênes et al. \(2017\)](#) also have revealed that in most of the sky, apart from the vicinity of the Galactic center, there are only single or double velocity components along the line of sight. Considering that $\sim 10\%$ of positions are covered by more than one cloud in the near velocities range of $(-30 25)$ km s^{-1} , the likelihood for our clouds, 95% of which have ^{12}CO velocity span less than 10 km s^{-1} , being projected together by multiple clouds on the line of sight is roughly 2%.

In numerical simulations, the relationship between the PPP density structures and PPV intensity structures has been explored in different aspects. In a simulated barred-spiral galaxy, [Pan et al. \(2015\)](#) found that $\sim 70\%$ of clouds had single counterparts in both PPP and PPV data sets. At the MC’s scale, [Beaumont et al. \(2013\)](#)

suggested that structures traced in ^{12}CO lines were more affected by overlap than those traced in ^{13}CO lines due to the opacity of ^{12}CO lines. The scaling relations, such as mass-size and size-linewidth, were found to be quite robust to projection by [Ballesteros-Paredes & Mac Low \(2002\)](#); [Beaumont et al. \(2013\)](#). In terms of velocity and density structures, [Pichardo et al. \(2000\)](#) reveal that the PPV features are more representative of the line of sight velocity than the density field. [Burkhart et al. \(2013\)](#) further found that the dominant structures in the PPP and PPV are strictly linked to supersonic gas. For our MC samples, which are extracted in the contiguous ^{12}CO emission in the PPV space of the Milky Way, we primarily focus on their internal velocity structures traced by the ^{13}CO emission. Their velocity dispersions are greater than $\sim 0.5 \text{ km s}^{-1}$, as listed in Table 2 of [Yuan et al. \(2023b\)](#). Comparing the sound speed $c_s = (kT_{\text{kin}}/\mu m_{\text{H}})^{1/2} \sim 0.2 \text{ km s}^{-1}$ for gas kinetic temperature $T_{\text{kin}}=10 \text{ K}$ and mean molecular weight $\mu=2.33$, thus these MC samples are thought to be supersonic. Therefore, based on these simulated results, the line of sight velocities of clouds are most likely represented by their velocity structures traced by the ^{13}CO lines.

4.2. Comparison with simulated works

The observed relative velocity between a pair of ^{13}CO structures is the absolute difference between the observed centroid velocity of each ^{13}CO structure, which is the three-dimensional (3D) velocity of each ^{13}CO structure ($\vec{V}_{3\text{D}}$) projected along the line of sight. We determine an angle of θ_j between the direction of $\vec{V}_{3\text{D},j}$ at the j th ^{13}CO structure and the line of sight, thus the ob-

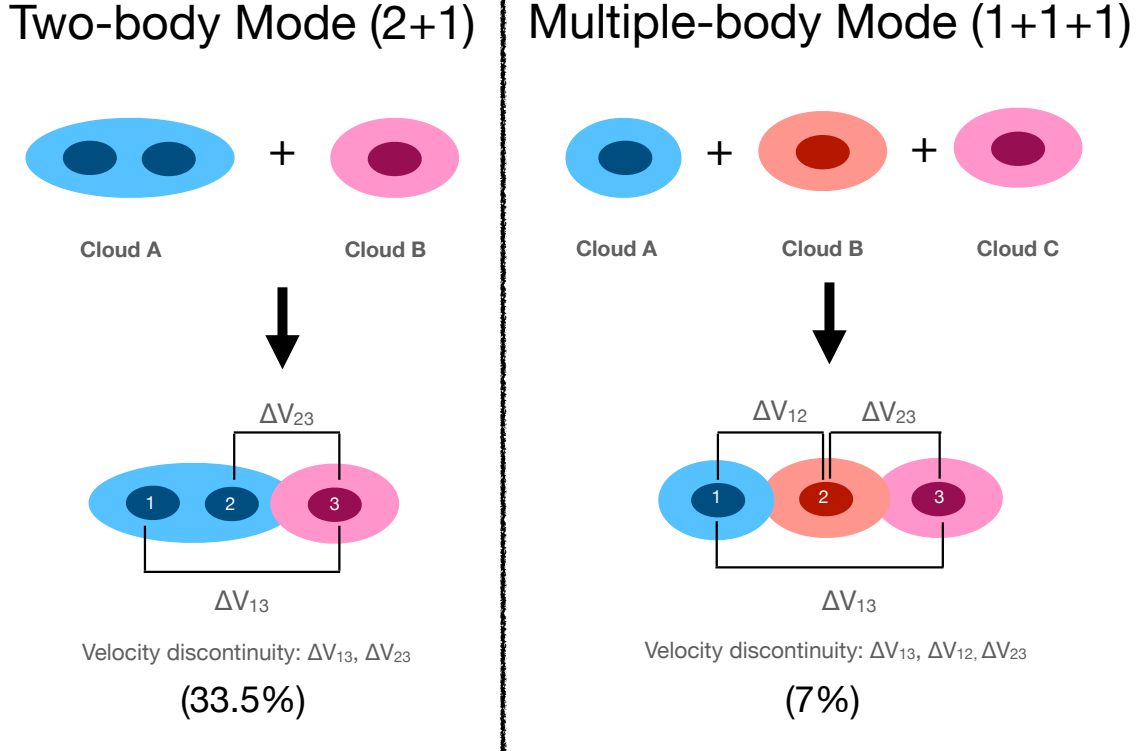


Figure 5. Schematic illustrations of the two kinds of combination modes for MCs with triple ^{13}CO structures.

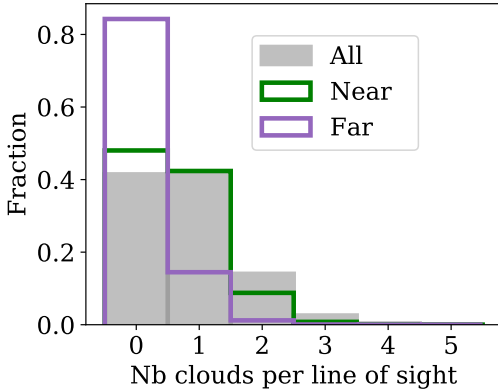


Figure 6. Histogram of the number of clouds along line of sight in each pixel. The y-axis is given in fractions of the total number of pixels in the region of $104^\circ.75 < l < 150^\circ.25$, $|b| < 5^\circ.25$. The ‘All’ means the line of sight with $-95 < V_{\text{LSR}} < 25 \text{ km s}^{-1}$, the ‘Near’ is along the line of sight with $-30 < V_{\text{LSR}} < 25 \text{ km s}^{-1}$, and the ‘Far’ is in a range of $-95 < V_{\text{LSR}} < -30 \text{ km s}^{-1}$.

served ΔV_{LOS} between j th and $(j-1)$ th ^{13}CO structure is $\Delta V_{\text{LOS}} = |V_{3\text{D},j} \cos \theta_j - V_{3\text{D},j-1} \cos \theta_{j-1}|$. While the relative velocity in 3D ($\Delta \vec{V}_{3\text{D}}$) between two ^{13}CO struc-

tures is $\Delta \vec{V}_{3\text{D}} = \vec{V}_{3\text{D},j} - \vec{V}_{3\text{D},j-1}$. We further assume a random distribution for the angle θ_j and get a mean value of $\langle \cos \theta_j \rangle = 1/\sqrt{2}$. Under these assumptions, we can roughly estimate the values of the relative velocities in 3D as $\Delta V_{3\text{D}} = \sqrt{2} \Delta V_{\text{LOS}}$. Our results indicate that over 95% of the $\Delta V_{3\text{D}}$ are less than 5 km s^{-1} , regardless of whether they are in the double or triple regime.

Based on our previous works, it appears that the distinct velocity discontinuities between ^{13}CO structures are most likely a result of cloud merging or splitting. In order to gain further insight into cloud motion and its relation to the internal ^{13}CO structure motion, it is necessary to systematically investigate cloud-cloud motion in further. Numerical simulations of the cloud’s motion can provide useful insight at this point. For instance, the distribution of relative velocities for the cloud-cloud collisions or mergers (CCCs) has been analyzed in a simulated galaxy (Horie et al. 2023). The distribution of the cloud collision speeds exhibits a similar trend to that of the observed relative velocities between internal ^{13}CO structures (Horie et al. 2023). However, the simulated values of cloud collision speeds are distributed at a peak of $\sim 7 \text{ km s}^{-1}$, with about 65% of them being less than 10 km s^{-1} (Horie et al. 2023). Nonetheless, Skarbinski

et al. (2023) have found that about 80% of mergers occur at a relative velocity of less than 5 km s^{-1} , implying that cloud mergers have a greater impact on aggregating mass into larger molecular complexes than generating shocks and further altering density structures of the merged cloud. This finding was also discussed in Dobbs et al. (2015); Jeffreson et al. (2021). In observation, Fukui et al. (2021) summarized the recent observational results on about 65 high-mass star-forming regions triggered by CCCs and found that their median collision velocity is $\sim 5 \text{ km s}^{-1}$. The distribution of internal relative velocities between ^{13}CO structures is fairly consistent with that for the merged speeds of clouds in these simulated works and observed results.

Furthermore, it is worth noting that the observed velocity discontinuities in this research are interpreted as the signatures of mergers or splits undergoing within MCs. However, we cannot exclude the possibilities of rotation motion, which likely arises from the turbulent flows from the shearing action of differential Galactic rotation (Fleck & Clark 1981; Belloche 2013; Arroyo-Chávez & Vázquez-Semadeni 2022). At least, our observed results also provide a constraint for the velocity gradients on the rotation motion of clouds. Additionally, further analysis on the distribution of the angular momentum from cloud scales down to internal substructures are helpful in resolving the process of the angular momentum redistribution within MCs.

5. CONCLUSIONS

Our study analyzes a sample of 443 ^{12}CO MCs with double ^{13}CO structures, and 185 ^{12}CO MCs with triple ^{13}CO structures from the MWISP CO survey. Our objective is to investigate the relative velocities on the line of sight between ^{13}CO structures (ΔV_{LOS}) within ^{12}CO clouds and identify the proportion of MCs exhibiting distinct velocity discontinuities. Our findings can be summarized as follows:

1. Approximately 70% of ΔV_{LOS} values are less than $\sim 1 \text{ km s}^{-1}$, and roughly 10% of values exceed 2 km s^{-1} with the maximum value reaching $\sim 5 \text{ km s}^{-1}$. For the ratios between ΔV_{LOS} values and internal velocity dispersions of ^{13}CO structures ($\Delta V_{\text{LOS}}/\sigma_{^{13}\text{CO},\text{in}}$), approximately 70% of them are less than 3 and about 10% are greater than 5, with several samples reaching ~ 12 .

2. The distributions of ΔV_{LOS} for MCs with double and triple ^{13}CO structures are similar, as well as their $\Delta V_{\text{LOS}}/\sigma_{^{13}\text{CO},\text{in}}$. Additionally, in the triple regime, distributions of ΔV_{LOS} between arbitrary two ^{13}CO structures and pairs of ^{13}CO structures connected by the minimal spanning tree are also similar. Such similarities suggest that the relative motions of ^{13}CO struc-

tures within clouds are random and regulated by the fundamental processes that are independent of structure complexities and cloud scales. Turbulent flows are a promising candidate, as they can be driven by dynamical processes in different scales.

3. About 40% of MCs in either double or triple regimes exhibit distinct velocity discontinuities, with relative velocities between ^{13}CO structures greater than the internal linewidths of ^{13}CO structures. The velocity fields for this portion of MC samples present redshifted and blueshifted velocities that come from the bulk motions of ^{13}CO structures.

4. Among the 40% of samples in the triple regime showing distinct velocity discontinuities, $\sim 33\%$ exhibit the signatures of bulk motions through the two-body motion, whereas the remaining $\sim 7\%$ show the features of combinations through the multiple-body motion. This suggests that cloud mergers or splits tend to occur between two MCs.

5. The indication of random motion among ^{13}CO structures and a considerable portion of distinct velocity discontinuities between ^{13}CO structures with ^{12}CO clouds provide further evidence for our previously proposed picture that ^{13}CO structures act as the building blocks of MCs, and the transient processes of MCs proceed by slow mergers or splits among these fundamental blocks.

This research made use of the data from the Milky Way Imaging Scroll Painting (MWISP) project, which is a multi-line survey in $^{12}\text{CO}/^{13}\text{CO}/\text{C}^{18}\text{O}$ along the northern galactic plane with PMO-13.7m telescope. We are grateful to all of the members of the MWISP working group, particularly the staff members at the PMO-13.7m telescope, for their long-term support. LY acknowledges Haoran Feng for his support on some data analysis scripts. This research was supported by the National Natural Science Foundation of China through grant 12303034 & 12041305 and the Natural Science Foundation of Jiangsu Province through grant BK20231104. MWISP was sponsored by the National Key R&D Program of China with grant 2023YFA1608000 & 2017YFA0402701 and the CAS Key Research Program of Frontier Sciences with grant QYZDJ-SSW-SLH047.

Data Availability. The extracted ^{12}CO line data for the 18,190 ^{12}CO clouds and the extracted ^{13}CO line data within the 2851 ^{12}CO clouds are publicly available at DOI:10.57760/sciencedb.j00001.00427.

Software: Astropy (Astropy Collaboration et al. 2013, 2018), Scipy (Virtanen et al. 2020), Matplotlib (Hunter 2007)

APPENDIX

A. BASIC PARAMETERS FOR MOLECULAR CLOUDS WITH DOUBLE AND TRIPLE ^{13}CO STRUCTURES

Figures A1 and A2 present distributions of angular areas, velocity spans, integrated fluxes, and peak intensities of ^{12}CO line emission for MC samples in the near and far groups, respectively.

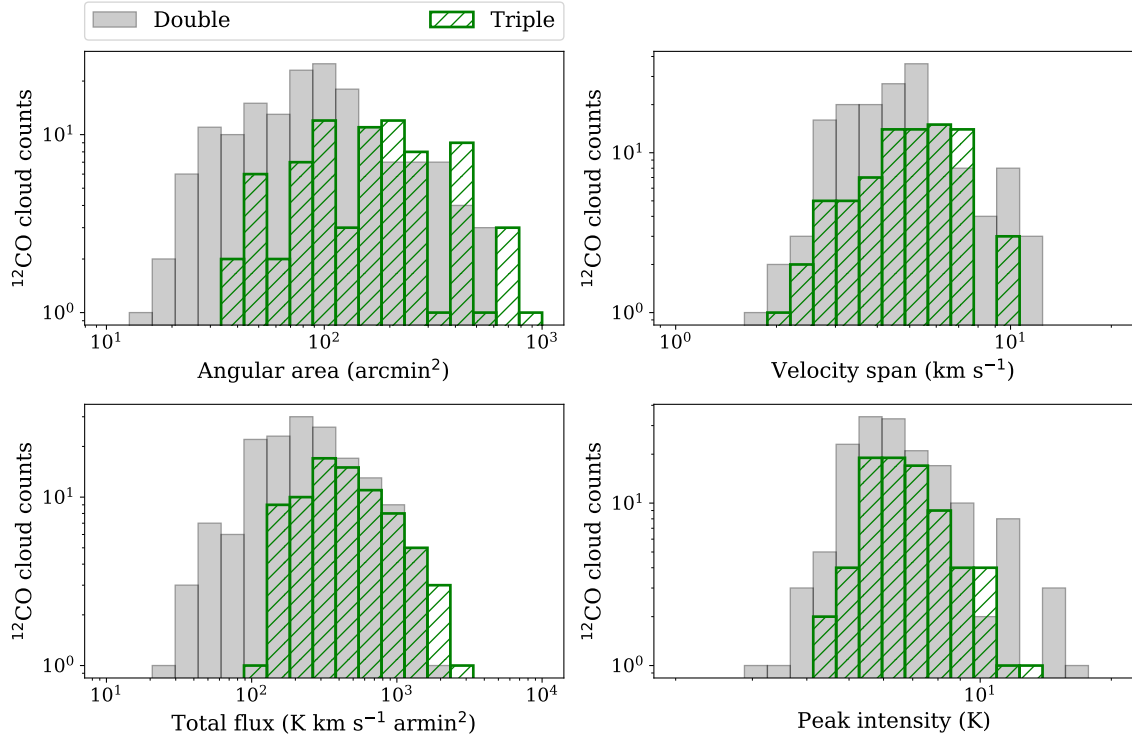


Figure A1. Number distributions of angular areas, velocity spans, integrated fluxes, and peak intensities of ^{12}CO line emission for MC samples in the near group. Most of these samples are located in the local arm and have kinematical distances of ~ 0.5 kpc. The gray histograms represent 163 ^{12}CO MCs with double ^{13}CO structures, and the green histograms represent 80 ^{12}CO MCs with triple ^{13}CO structures.

B. MOLECULAR CLOUDS WITH DISTINCT VELOCITY DISCONTINUITIES

Figure B1 shows velocity fields for MC samples with double ^{13}CO structures, which display distinct velocity discontinuities. Figures B2 and B3 present velocity fields for MC samples with triple ^{13}CO structures, which are identified to have distinct velocity discontinuities.

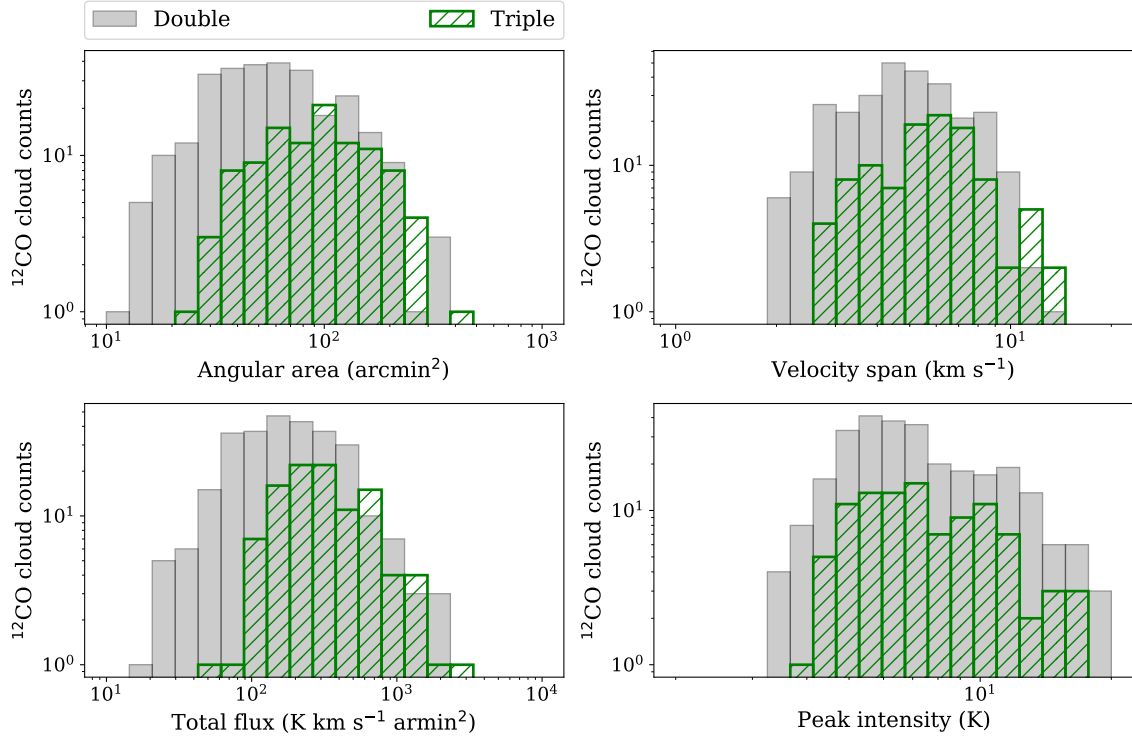


Figure A2. Number distribution of angular areas, velocity spans, integrated fluxes, and peak intensities of ^{12}CO line emission for MC samples in the far group, most of which are distributed in the Perseus arm with kinematical distances of ~ 2 kpc. The gray histograms represent 280 ^{12}CO MCs with double ^{13}CO structures, and the green histograms represent 105 ^{12}CO MCs with triple ^{13}CO structures.

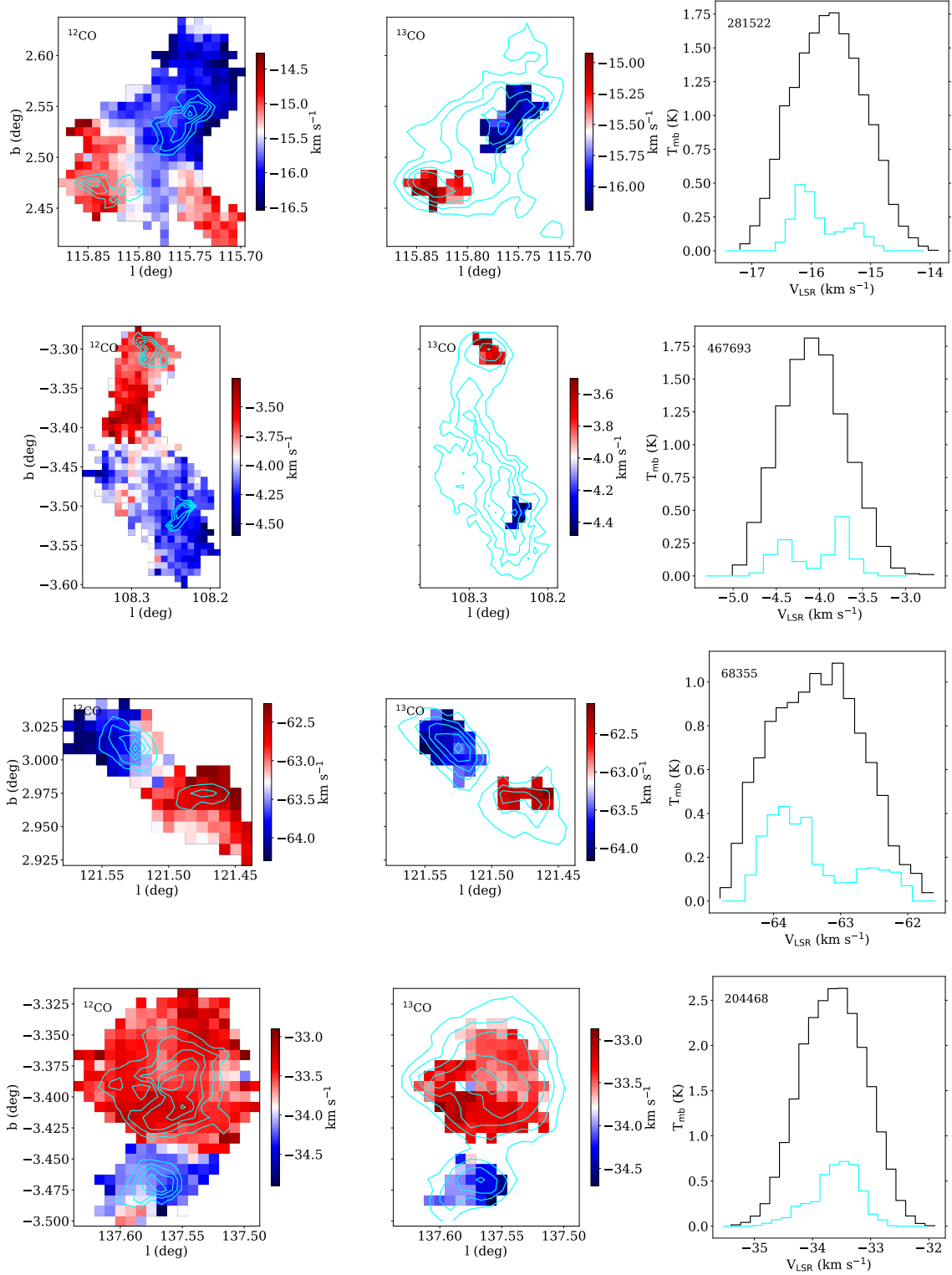


Figure B1. Velocity fields of MCs with double ^{13}CO structures, whose relative velocities are characterized as distinct velocity discontinuities. **Left panel:** the color map represents the first moment map (velocity field) of ^{12}CO emission of MCs, and the cyan contours show the moment zero map (velocity-integrated intensity) of ^{13}CO line emission, ranging from 10% to 90% in increments of 20% of its maximum value. **Middle panel:** the color map represents the first moment map (velocity field) of ^{13}CO emission of MCs, and the cyan contours show the moment zero map (velocity-integrated intensity) of ^{12}CO line emission, ranging from 10% to 90% in increments of 20% of its maximum value. **Right panel:** the averaged spectral lines for the extracted ^{12}CO line emission (black) and ^{13}CO line emission (cyan) within MCs. The number noted in the upper-left corner is the number ID for MC samples.

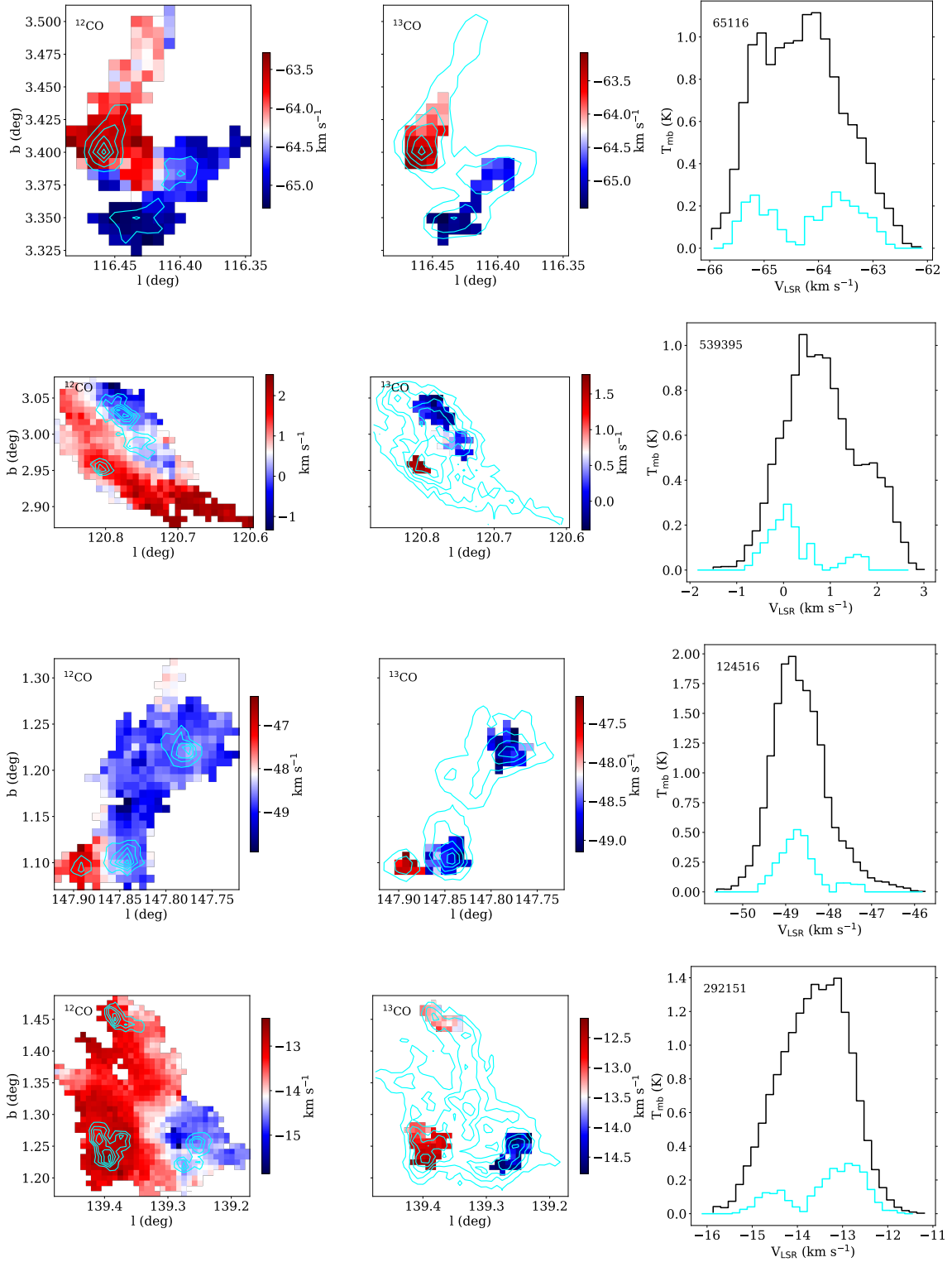


Figure B2. Same as Figure B1, but for the MC with triple ^{13}CO structures, where two distinct velocity discontinuities between each two of ^{13}CO structures are determined.

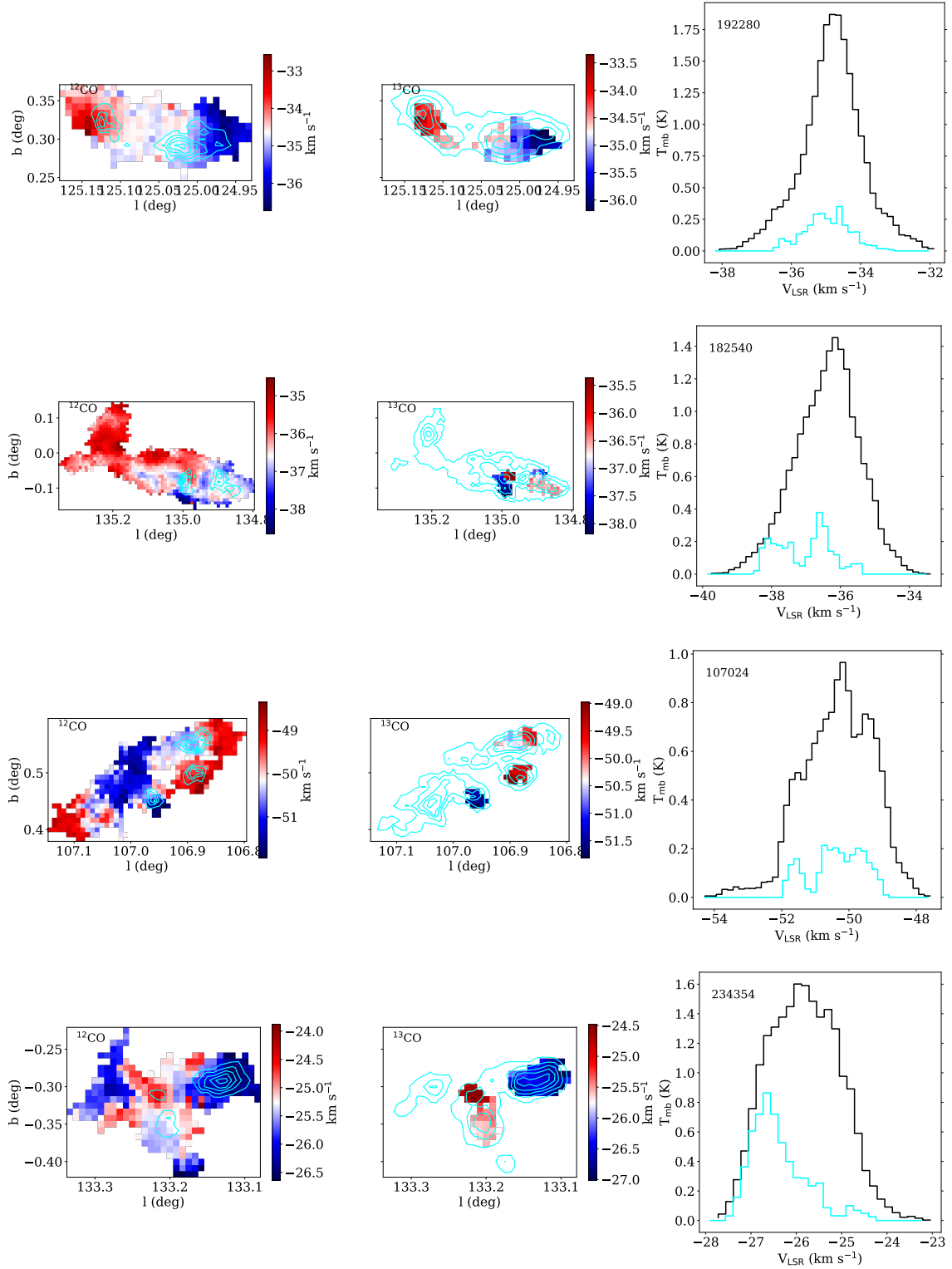


Figure B3. Same as Figure B1, but for the MC with triple ^{13}CO structures, where three distinct velocities discontinuities between each two of ^{13}CO structures are determined.

REFERENCES

- André, P., Di Francesco, J., Ward-Thompson, D., et al. 2014, in *Protostars and Planets VI*, ed. H. Beuther, R. S. Klessen, C. P. Dullemond, & T. Henning, 27, doi: [10.2458/azu_uapress_9780816531240-ch002](https://doi.org/10.2458/azu_uapress_9780816531240-ch002)
- André, P., Men'shchikov, A., Bontemps, S., et al. 2010, *A&A*, 518, L102, doi: [10.1051/0004-6361/201014666](https://doi.org/10.1051/0004-6361/201014666)
- Arroyo-Chávez, G., & Vázquez-Semadeni, E. 2022, *ApJ*, 925, 78, doi: [10.3847/1538-4357/ac3915](https://doi.org/10.3847/1538-4357/ac3915)
- Astropy Collaboration, Robitaille, T. P., Tollerud, E. J., et al. 2013, *A&A*, 558, A33, doi: [10.1051/0004-6361/201322068](https://doi.org/10.1051/0004-6361/201322068)
- Astropy Collaboration, Price-Whelan, A. M., Sipőcz, B. M., et al. 2018, *AJ*, 156, 123, doi: [10.3847/1538-3881/aabc4f](https://doi.org/10.3847/1538-3881/aabc4f)
- Ballesteros-Paredes, J., & Mac Low, M.-M. 2002, *ApJ*, 570, 734, doi: [10.1086/339624](https://doi.org/10.1086/339624)
- Ballesteros-Paredes, J., Vázquez-Semadeni, E., & Scalo, J. 1999a, *ApJ*, 515, 286, doi: [10.1086/307007](https://doi.org/10.1086/307007)
- . 1999b, *ApJ*, 515, 286, doi: [10.1086/307007](https://doi.org/10.1086/307007)
- Ballesteros-Paredes, J., André, P., Hennebelle, P., et al. 2020, *SSRv*, 216, 76, doi: [10.1007/s11214-020-00698-3](https://doi.org/10.1007/s11214-020-00698-3)
- Beaumont, C. N., Offner, S. S. R., Shetty, R., Glover, S. C. O., & Goodman, A. A. 2013, *ApJ*, 777, 173, doi: [10.1088/0004-637X/777/2/173](https://doi.org/10.1088/0004-637X/777/2/173)
- Belloche, A. 2013, in *EAS Publications Series*, Vol. 62, *EAS Publications Series*, ed. P. Hennebelle & C. Charbonnel, 25–66, doi: [10.1051/eas/1362002](https://doi.org/10.1051/eas/1362002)
- Beuther, H., Wang, Y., Soler, J., et al. 2020, *A&A*, 638, A44, doi: [10.1051/0004-6361/202037950](https://doi.org/10.1051/0004-6361/202037950)
- Bonnell, I. A., Dobbs, C. L., Robitaille, T. P., & Pringle, J. E. 2006, *MNRAS*, 365, 37, doi: [10.1111/j.1365-2966.2005.09657.x](https://doi.org/10.1111/j.1365-2966.2005.09657.x)
- Brunt, C. M., Heyer, M. H., & Mac Low, M. M. 2009, *A&A*, 504, 883, doi: [10.1051/0004-6361/200911797](https://doi.org/10.1051/0004-6361/200911797)
- Burkhart, B., Lazarian, A., Goodman, A., & Rosolowsky, E. 2013, *ApJ*, 770, 141, doi: [10.1088/0004-637X/770/2/141](https://doi.org/10.1088/0004-637X/770/2/141)
- Chandrasekhar, S., & Fermi, E. 1953, *ApJ*, 118, 113, doi: [10.1086/145731](https://doi.org/10.1086/145731)
- Dame, T. M., Elmegreen, B. G., Cohen, R. S., & Thaddeus, P. 1986, *ApJ*, 305, 892, doi: [10.1086/164304](https://doi.org/10.1086/164304)
- Dobbs, C. L., & Bonnell, I. A. 2008, *MNRAS*, 385, 1893, doi: [10.1111/j.1365-2966.2008.12995.x](https://doi.org/10.1111/j.1365-2966.2008.12995.x)
- Dobbs, C. L., Burkert, A., & Pringle, J. E. 2011, *MNRAS*, 417, 1318, doi: [10.1111/j.1365-2966.2011.19346.x](https://doi.org/10.1111/j.1365-2966.2011.19346.x)
- Dobbs, C. L., & Pringle, J. E. 2013, *MNRAS*, 432, 653, doi: [10.1093/mnras/stt508](https://doi.org/10.1093/mnras/stt508)
- Dobbs, C. L., Pringle, J. E., & Duarte-Cabral, A. 2015, *MNRAS*, 446, 3608, doi: [10.1093/mnras/stu2319](https://doi.org/10.1093/mnras/stu2319)
- Ester, M., Kriegel, H.-P., Sander, J., & Xu, X. 1996, in *Proceedings of the Second International Conference on Knowledge Discovery and Data Mining, KDD'96 (AAAI Press)*, 226–231, <http://dl.acm.org/citation.cfm?id=3001460.3001507>
- Field, G. B. 1965, *ApJ*, 142, 531, doi: [10.1086/148317](https://doi.org/10.1086/148317)
- Fleck, R. C., J., & Clark, F. O. 1981, *ApJ*, 245, 898, doi: [10.1086/158866](https://doi.org/10.1086/158866)
- Fukui, Y., Habe, A., Inoue, T., Enokiya, R., & Tachihara, K. 2021, *PASJ*, 73, S1, doi: [10.1093/pasj/psaa103](https://doi.org/10.1093/pasj/psaa103)
- Fukui, Y., Torii, K., Ohama, A., et al. 2016, *ApJ*, 820, 26, doi: [10.3847/0004-637X/820/1/26](https://doi.org/10.3847/0004-637X/820/1/26)
- Fukui, Y., Ohama, A., Kohno, M., et al. 2018, *PASJ*, 70, S46, doi: [10.1093/pasj/psy005](https://doi.org/10.1093/pasj/psy005)
- Goldreich, P., & Lynden-Bell, D. 1965, *MNRAS*, 130, 97, doi: [10.1093/mnras/130.2.97](https://doi.org/10.1093/mnras/130.2.97)
- Gong, Y., Fang, M., Mao, R., et al. 2017, *ApJL*, 835, L14, doi: [10.3847/2041-8213/835/1/L14](https://doi.org/10.3847/2041-8213/835/1/L14)
- Heitsch, F., Slyz, A. D., Devriendt, J. E. G., Hartmann, L. W., & Burkert, A. 2006, *ApJ*, 648, 1052, doi: [10.1086/505931](https://doi.org/10.1086/505931)
- Henshaw, J. D., Kruijssen, J. M. D., Longmore, S. N., et al. 2020, *Nature Astronomy*, 4, 1064, doi: [10.1038/s41550-020-1126-z](https://doi.org/10.1038/s41550-020-1126-z)
- Heyer, M., Krawczyk, C., Duval, J., & Jackson, J. M. 2009, *ApJ*, 699, 1092, doi: [10.1088/0004-637X/699/2/1092](https://doi.org/10.1088/0004-637X/699/2/1092)
- Heyer, M. H., & Brunt, C. M. 2004, *ApJL*, 615, L45, doi: [10.1086/425978](https://doi.org/10.1086/425978)
- Heyer, M. H., Williams, J. P., & Brunt, C. M. 2006, *ApJ*, 643, 956, doi: [10.1086/503096](https://doi.org/10.1086/503096)
- Horie, S., Okamoto, T., & Habe, A. 2023, *arXiv e-prints*, arXiv:2311.04175, doi: [10.48550/arXiv.2311.04175](https://doi.org/10.48550/arXiv.2311.04175)
- Hunter, J. D. 2007, *Computing in Science & Engineering*, 9, 90, doi: [10.1109/MCSE.2007.55](https://doi.org/10.1109/MCSE.2007.55)
- Jeffreson, S. M. R., Keller, B. W., Winter, A. J., et al. 2021, *MNRAS*, 505, 1678, doi: [10.1093/mnras/stab1293](https://doi.org/10.1093/mnras/stab1293)
- Jeffreson, S. M. R., Semenov, V. A., & Krumholz, M. R. 2024, *MNRAS*, 527, 7093, doi: [10.1093/mnras/stad3550](https://doi.org/10.1093/mnras/stad3550)
- Kim, C.-G., Kim, W.-T., & Ostriker, E. C. 2006, *ApJL*, 649, L13, doi: [10.1086/508160](https://doi.org/10.1086/508160)
- Koyama, H., & Inutsuka, S.-I. 2000, *ApJ*, 532, 980, doi: [10.1086/308594](https://doi.org/10.1086/308594)
- Krumholz, M. R., Matzner, C. D., & McKee, C. F. 2006, *ApJ*, 653, 361, doi: [10.1086/508679](https://doi.org/10.1086/508679)
- Larson, R. B. 1981, *MNRAS*, 194, 809, doi: [10.1093/mnras/194.4.809](https://doi.org/10.1093/mnras/194.4.809)
- Li, G.-X., & Burkert, A. 2018, *MNRAS*, 474, 2167, doi: [10.1093/mnras/stx2827](https://doi.org/10.1093/mnras/stx2827)

- Lin, C. C., & Shu, F. H. 1964, *ApJ*, 140, 646, doi: [10.1086/147955](https://doi.org/10.1086/147955)
- Ma, Y., Wang, H., Li, C., et al. 2021, *ApJS*, 254, 3, doi: [10.3847/1538-4365/abe85c](https://doi.org/10.3847/1538-4365/abe85c)
- Ma, Y., Wang, H., Zhang, M., et al. 2022, *ApJS*, 262, 16, doi: [10.3847/1538-4365/ac7797](https://doi.org/10.3847/1538-4365/ac7797)
- Mac Low, M.-M., & Klessen, R. S. 2004, *Reviews of Modern Physics*, 76, 125, doi: [10.1103/RevModPhys.76.125](https://doi.org/10.1103/RevModPhys.76.125)
- McKee, C. F. 1989, *ApJ*, 345, 782, doi: [10.1086/167950](https://doi.org/10.1086/167950)
- Miville-Deschênes, M.-A., Murray, N., & Lee, E. J. 2017, *ApJ*, 834, 57, doi: [10.3847/1538-4357/834/1/57](https://doi.org/10.3847/1538-4357/834/1/57)
- Molinari, S., Swinyard, B., Bally, J., et al. 2010, *A&A*, 518, L100, doi: [10.1051/0004-6361/201014659](https://doi.org/10.1051/0004-6361/201014659)
- Myers, P. C. 1983, *ApJ*, 270, 105, doi: [10.1086/161101](https://doi.org/10.1086/161101)
- Myers, P. C., & Goodman, A. A. 1988, *ApJL*, 326, L27, doi: [10.1086/185116](https://doi.org/10.1086/185116)
- Pan, H.-A., Fujimoto, Y., Tasker, E. J., et al. 2015, *MNRAS*, 453, 3082, doi: [10.1093/mnras/stv1843](https://doi.org/10.1093/mnras/stv1843)
- Passot, T., Vázquez-Semadeni, E., & Pouquet, A. 1995, *ApJ*, 455, 536, doi: [10.1086/176603](https://doi.org/10.1086/176603)
- Pichardo, B., Vázquez-Semadeni, E., Gazol, A., Passot, T., & Ballesteros-Paredes, J. 2000, *ApJ*, 532, 353, doi: [10.1086/308546](https://doi.org/10.1086/308546)
- Rani, R., Moore, T. J. T., Eden, D. J., et al. 2023, *MNRAS*, 523, 1832, doi: [10.1093/mnras/stad1507](https://doi.org/10.1093/mnras/stad1507)
- Reid, M. J., Dame, T. M., Menten, K. M., & Brunthaler, A. 2016, *ApJ*, 823, 77, doi: [10.3847/0004-637X/823/2/77](https://doi.org/10.3847/0004-637X/823/2/77)
- Reid, M. J., Menten, K. M., Brunthaler, A., et al. 2019, *ApJ*, 885, 131, doi: [10.3847/1538-4357/ab4a11](https://doi.org/10.3847/1538-4357/ab4a11)
- Rice, T. S., Goodman, A. A., Bergin, E. A., Beaumont, C., & Dame, T. M. 2016, *ApJ*, 822, 52, doi: [10.3847/0004-637X/822/1/52](https://doi.org/10.3847/0004-637X/822/1/52)
- Riener, M., Kainulainen, J., Beuther, H., et al. 2020, *A&A*, 633, A14, doi: [10.1051/0004-6361/201936814](https://doi.org/10.1051/0004-6361/201936814)
- Roman-Duval, J., Jackson, J. M., Heyer, M., Rathborne, J., & Simon, R. 2010, *ApJ*, 723, 492, doi: [10.1088/0004-637X/723/1/492](https://doi.org/10.1088/0004-637X/723/1/492)
- Shan, W., Yang, J., Shi, S., et al. 2012, *IEEE Transactions on Terahertz Science and Technology*, 2, 593, doi: [10.1109/TTHZ.2012.2213818](https://doi.org/10.1109/TTHZ.2012.2213818)
- Shu, F. H., Adams, F. C., & Lizano, S. 1987, *ARA&A*, 25, 23, doi: [10.1146/annurev.aa.25.090187.000323](https://doi.org/10.1146/annurev.aa.25.090187.000323)
- Silk, J. 1985, *ApJL*, 292, L71, doi: [10.1086/184475](https://doi.org/10.1086/184475)
- Skarbinski, M., Jeffreson, S. M. R., & Goodman, A. A. 2023, *MNRAS*, 519, 1887, doi: [10.1093/mnras/stac3627](https://doi.org/10.1093/mnras/stac3627)
- Solomon, P. M., Rivolo, A. R., Barrett, J., & Yahil, A. 1987, *ApJ*, 319, 730, doi: [10.1086/165493](https://doi.org/10.1086/165493)
- Su, Y., Yang, J., Zhang, S., et al. 2019, *ApJS*, 240, 9, doi: [10.3847/1538-4365/aaf1c8](https://doi.org/10.3847/1538-4365/aaf1c8)
- Tasker, E. J., & Tan, J. C. 2009, *ApJ*, 700, 358, doi: [10.1088/0004-637X/700/1/358](https://doi.org/10.1088/0004-637X/700/1/358)
- Traficante, A., Fuller, G. A., Duarte-Cabral, A., et al. 2020, *MNRAS*, 491, 4310, doi: [10.1093/mnras/stz3344](https://doi.org/10.1093/mnras/stz3344)
- Vázquez-Semadeni, E. 1994, *ApJ*, 423, 681, doi: [10.1086/173847](https://doi.org/10.1086/173847)
- Vázquez-Semadeni, E., Banerjee, R., Gómez, G. C., et al. 2011, *MNRAS*, 414, 2511, doi: [10.1111/j.1365-2966.2011.18569.x](https://doi.org/10.1111/j.1365-2966.2011.18569.x)
- Vázquez-Semadeni, E., Gómez, G. C., Jappsen, A. K., et al. 2007, *ApJ*, 657, 870, doi: [10.1086/510771](https://doi.org/10.1086/510771)
- Vázquez-Semadeni, E., Passot, T., & Pouquet, A. 1995, *ApJ*, 441, 702, doi: [10.1086/175393](https://doi.org/10.1086/175393)
- Virtanen, P., Gommers, R., Oliphant, T. E., et al. 2020, *Nature Methods*, 17, 261, doi: [10.1038/s41592-019-0686-2](https://doi.org/10.1038/s41592-019-0686-2)
- Wada, K., Meurer, G., & Norman, C. A. 2002, *ApJ*, 577, 197, doi: [10.1086/342151](https://doi.org/10.1086/342151)
- Watkins, E. J., Barnes, A. T., Henny, K., et al. 2023, *ApJL*, 944, L24, doi: [10.3847/2041-8213/aca6e4](https://doi.org/10.3847/2041-8213/aca6e4)
- Xu, Y., Hao, C. J., Liu, D. J., et al. 2023, *ApJ*, 947, 54, doi: [10.3847/1538-4357/acc45c](https://doi.org/10.3847/1538-4357/acc45c)
- Yan, Q.-Z., Yang, J., Su, Y., Sun, Y., & Wang, C. 2020, *ApJ*, 898, 80, doi: [10.3847/1538-4357/ab9f9c](https://doi.org/10.3847/1538-4357/ab9f9c)
- Yan, Q.-Z., Yang, J., Sun, Y., et al. 2021, *A&A*, 645, A129, doi: [10.1051/0004-6361/202039768](https://doi.org/10.1051/0004-6361/202039768)
- Yan, Q.-Z., Yang, J., Su, Y., et al. 2022, *AJ*, 164, 55, doi: [10.3847/1538-3881/ac77ea](https://doi.org/10.3847/1538-3881/ac77ea)
- Yuan, L., Li, G.-X., Zhu, M., et al. 2020, *A&A*, 637, A67, doi: [10.1051/0004-6361/201936625](https://doi.org/10.1051/0004-6361/201936625)
- Yuan, L., Yang, J., Du, F., et al. 2021, *ApJS*, 257, 51, doi: [10.3847/1538-4365/ac242a](https://doi.org/10.3847/1538-4365/ac242a)
- . 2022, *ApJS*, 261, 37, doi: [10.3847/1538-4365/ac739f](https://doi.org/10.3847/1538-4365/ac739f)
- . 2023a, *ApJ*, 944, 91, doi: [10.3847/1538-4357/acac26](https://doi.org/10.3847/1538-4357/acac26)
- . 2023b, *ApJ*, 958, 7, doi: [10.3847/1538-4357/acf9ef](https://doi.org/10.3847/1538-4357/acf9ef)